The Crystal Structure of Phosphoribulokinase from *Rhodobacter sphaeroides* Reveals a Fold Similar to That of Adenylate Kinase[†]

David H. T. Harrison,* Jennifer A. Runquist, Alison Holub, and Henry M. Miziorko

Department of Biochemistry, Medical College of Wisconsin, Milwaukee, Wisconsin 53226

Received November 17, 1997; Revised Manuscript Received January 30, 1998

ABSTRACT: The essential photosynthetic enzyme phosphoribulokinase (PRK) is responsible for the conversion of ribulose 5-phosphate (Ru5P) to ribulose 1,5-bisphosphate, the substrate for the CO_2 fixing enzyme ribulose 1,5-bisphosphate carboxylase/oxygenase (Rubisco). We have determined the structure of the octameric bacterial form of PRK to a resolution of 2.5 Å. The protein is folded into a seven-member mixed β-sheet surrounded by α-helices, giving the overall appearance of the nucleotide monophosphate family of kinases. Homology with the nucleotide monophosphate kinases suggests a number of amino acid residues that are likely to be important in catalysis and suggests the roles of some amino acid residues that have been mutated prior to the determination of the structure. Further, sequence identity across eukaryotic and prokaryotic species and a calculation of the buried surface area suggests the identity within the octamer of a dimer conserved throughout evolution. The width of the groove leading to the active site is consistent with an oriented molecule of thioredoxin controlling the oxidation state of two cysteines that regulate activity in the eukaryotic enzymes. Although neither Asp 42 nor Asp 169 can be definitively assigned as the catalytic base, the crystal structure suggests the location of a ribulose 5-phosphate binding site and suggests a role for several of the conserved basic residues.

The synthesis of ribulose 1,5-bisphosphate (RuBP)[1] by phosphoribulokinase (PRK; EC 2.7.1.19) is essential for the creation of all new biomass (e.g., sugars, proteins, lipids) in the biosphere. PRK catalyzes an in-line phosphoryl transfer (*1*) from magnesium adenosine triphosphate (Mg·ATP) to ribulose 5-phosphate (Ru5P) to form magnesium adenosine diphosphate (Mg·ADP) and ribulose 1,5-bisphosphate (RuBP), the CO_2 acceptor in Calvin's reductive pentose phosphate cycle. The quaternary structures and regulatory properties of PRK from different organisms can be divided along prokaryotic and eukaryotic lines. Most prokaryotic PRKs exist as octamers of 32-kDa subunits (*2*) and are subject to allosteric regulation (*3*). Eukaryotic PRKs are dimers of about 40 kDa and are regulated by reversible oxidation/reduction of cysteine sulfhydryls (*4*). The sequence identity between all PRKs is about 10%, with sequence identities within a kingdom of greater than 25%.

Despite differences in quaternary structure, regulatory mechanism, and overall sequence identity, the available chemical and mutagenic data suggest that the active sites of both the bacterial PRK and the plant PRK will be similar. The N-terminal portion of the plant PRK has been affinity-labeled by a reactive ATP analogue (*5*, *6*). The N-terminal portion of the molecule contains a P-loop or "Walker A" sequence (residues 12−20) that is associated with NTP binding in NTP binding proteins (*7*). Residues in this structure form a loop between a strand and a helix that may bind to the β and γ phosphoryls of ATP. Site-directed mutagenesis of the two regulatory sulfhydryls in the eukaryotic PRK (i.e., Cys-16 and Cys-55) shows that neither is required for catalysis (*8*). Further, mutagenesis of a number of absolutely conserved basic and acidic residues show dramatic changes in either k_{cat} or K_m for the two substrates (*9−11*). Unlike nucleotide monophosphate kinases, phosphosugar kinases such as PRK and 6-phosphofructo-2-kinase (F6P 2K) are required to deprotonate the phosphoryl acceptor for efficient phosphorylation to occur. Mutagenesis studies implicated either Asp42 or Asp169 as the catalytic base that activates the O1 hydroxyl oxygen for nucleophilic attack on the γ-phosphoryl of ATP. The other aspartic acid has been assumed to act as a ligand for the Mg^{2+} ion. Other important amino acids found by a phylogenetic approach to mutagenesis include residues His 45, Arg 49, Arg 168, and Arg 173, which are all implicated in Ru5P binding.

To understand the three-dimensional relationship of these and other catalytic residues and to determine the relationship between the eukaryotic and prokaryotic forms of the enzyme, we have determined the three-dimensional structure of phosphoribulokinase from *Rhodobacter sphaeroides*.

METHODS AND MATERIALS

Protein Expression and Purification. Recombinant PRK from *Rb. sphaeroides* was expressed in pETbprkwt transformed BL21(DE3) *Escherichia coli* cells. These cells were grown, induced, and harvested according to Charlier et al. (*9*). Protein purification also proceeded according to Charlier et al. (*9*) with the following modifications. The crude lysate

---

[1] Abbreviations: PRK, phosphoribulokinase; Ru5P, ribulose 5-phosphate; RuBP, ribulose 1,5-bisphosphate; PFK, phosphofructokinase; F6P 2K, 6-phosphofructo-2-kinase.

was dialyzed against buffer (25 mM Tris, pH 8.2, 1 mM EDTA, and 10 mM β-mercaptoethanol) and loaded on a Fast-Q (Pharmacia) anion exchange column. A 1-L linear gradient of KCl (0−0.6 M) was used to elute the protein (~0.2 M KCl) from the column. The protein was dialyzed and loaded batchwise on an agarose-reactive Green 19 column. Purified PRK was eluted with 10 mM ATP, dialyzed against buffer (25 mM Tris, pH 8.2), and diluted to 7 mg/mL for crystallization.

Crystallization. PRK crystals were formed as reported earlier (*12*) with the exception that ammonium sulfate was substituted for ammonium phosphate. The resulting crystals (best grown at a temperature of 19 °C) were isomorphous with the original crystals (cubic space group *P*432, *a* = 129.6), although the morphology was changed to an irregular polyhedron, instead of the cubic morphology originally described. These crystals could be grown reproducibly to a size of more than 0.3 mm in any dimension. Like the original crystals, these crystals are very fragile and cannot be stabilized in an artificial mother liquor.

Data Collection. PRK crystals (0.3 mm on a side) mounted in oil-sealed 0.7 mm diameter quartz capillaries were centered in a two-circle Rigaku R-axis II image plate detector system and exposed to 0.3 mm collimated graphite monochromatized Cu Kα radiation generated from a Rigaku RU-200 rotating anode X-ray generator at 50 kV × 100 mA. Rotation photographs (1.2°) were taken with the crystal to detector distance set to 140 mm. Image data were processed (integrated, corrected, and scaled) with the HKL program suite (*13*).

Heavy Atom Derivatives. One microliter of a 10 mM thimerosal solution was added to a 10 μL drop containing one or more PRK crystals. Alternatively, a grain of $K_2Pt(CN)_4$ was added to a 10 μL drop containing one or more PRK crystals. The crystal containing drops were then placed in an oil-sealed chamber containing the original well solution. After 3 h, a crystal was selected for X-ray diffraction. R_{merge} values for the mercury and platinum derivatives were 7.3% and 7.7%; the isomorphous differences were about 24% and 15%, respectively.

Computations and Computer Graphics. Interpretation and computation of Patterson maps and initial heavy atom refinement was aided by the use of the XTALVIEW (*14*) program suite. The CCP4 program suite (*15*) was used for subsequent heavy atom refinement and solvent flattening. Model generation and manual fitting of an atomic model to electron density maps was performed with the program O (*16*) on an Indigo II Silicon Graphics workstation. The model was refined using both simulated annealing and constrained least-squares refinement by the program XPLOR (*17*).

RESULTS

Locating the Heavy Atom Sites. Calculation of the mercury isomorphous difference Patterson map revealed peaks in the Harker section (*u*, 0, *w*) consistent with a mercury site at (0.479, 0.105, 0.154) or its enantiomorph (0.479, 0.154, 0.105). This site was found with an automated Patterson interpretation program within the XTALVIEW suite (XHERCULES) and the position was checked by using

Table 1

	native	thimerosal (Hg)	platinum cyanide (Pt)
resolution (Å)	30−2.5	30−3.0	30−3.0
no. of reflections observed ($I > 1\sigma$)	42132	24803	17446
no. of reflections unique ($I > 2\sigma$)	10956	6881	6400
% complete ($I > 2\sigma$)	80.6	85.1	80.4
R_{merge} ($I > 2\sigma$) (%)	6.2	7.3	7.7

heavy atom sites	*x*	*y*	*z*	occ/*B*
Hg	0.479	0.105	0.154	0.067/52
Pt (1)	0.017	0.142	0.362	0.014/5
Pt (2)	0.141	0.434	0.349	0.016/45
Pt (3)	0.038	0.278	0.396	0.007/45

resolution (Å)	thimerosal phasing power (acentric)	$K_2Pt(CN)_4$ phasing power (acentric)	combined figure of merit (all) unflattened	combined figure of merit (all) flattened
7.5	2.42	0.94	0.729	0.844
6	2.59	1.11	0.691	0.786
5	2.16	1.11	0.631	0.772
4.3	1.39	1.06	0.532	0.693
3.75	1.08	0.95	0.454	0.678
3.33	0.94	0.94	0.376	0.651
3	0.78	0.8	0.297	0.619
overall (no. of refs)	1.23 (6000)	0.94 (6025)	0.463 (7780)	

the program XPATPRED. An anomalous difference Patterson map was calculated and shows many of the same features found in the isomorphous difference map. The position and occupancy of the mercury site was refined, and single isomorphous replacement (SIR) phases were generated. These phases were used to calculate a platinum isomorphous difference Fourier map with $F_{Pt} - F_{nat}$ as coefficients. The map showed two peaks that were consistent with the platinum isomorphous difference Patterson map and one peak that did not appear in the Harker section but did account for some of the "cross-peaks" in the map. The positions and occupancies of the three platinum sites were refined and phases calculated by using these sites were used in a Fourier synthesis with $F_{Hg} - F_{nat}$ as coefficients. The resulting mercury isomorphous difference Fourier map showed electron density at the mercury site, which validated the usefulness of the platinum sites. The platinum anomalous differences were insufficient to be used in phasing calculations. The correct hand of the mercury anomalous signal was determined by observing the differences in the strength of the platinum Fourier peaks by using phases calculated without anomalous data, with the positive or negative hand of the anomalous data.

Refinement of the heavy atom sites and occupancies confirmed that the mercury derivative is much "stronger" as revealed by its phasing power (Table 1). The overall figure of merit to 3.5 Å was 0.59 and the overall figure of merit to 3.0 Å was 0.46. To improve the phases, we took advantage of the fact that 54% of the crystal is composed of solvent. Solvent flattening (program DM, *15*) produced an overall figure of merit of 0.72 for the phases to a resolution of 3.0 Å. These solvent-flattened phases were used to generate a Fourier map with F_{obs} as coefficients. This map revealed electron density that could be readily categorized as either β-sheet or α-helix.

Building the Atomic Model. A polyalanine chain was built into the solvent flattened MIR map at either 3.5 Å or 3.0 Å

Table 2: Crystallographic Refinement Data for the Structure of Phosphoribulokinase[a]

resolution range (Å)	working R-value				free R-value			
	no. of refls	% comp	shell	accum	no. of refls	% comp	shell	accum
4.95−15.0	1567	82.5	0.222	0.222	70	3.6	0.324	0.323
3.95−4.95	1504	87.4	0.163	0.194	83	4.9	0.223	0.270
3.46−3.95	1403	83.8	0.194	0.194	85	5.0	0.286	0.275
3.14−3.46	1352	81.1	0.208	0.196	72	4.3	0.276	0.275
2.92−3.14	1309	79.1	0.235	0.200	57	3.4	0.304	0.278
2.75−2.92	1171	71.6	0.262	0.205	61	3.7	0.330	0.282
2.61−2.75	1074	65.8	0.281	0.209	59	3.6	0.313	0.284
2.50−2.61	916	56.2	0.298	0.213	45	2.7	0.298	0.284
2.50−15.0	10296	76.2		0.213	532	3.9		0.284

rms deviation from idealty		
bond lengths	0.013	43 water atoms
bond angles	1.337	5 sulfate atoms
dihedral angles	27.640	2203 protein atoms (282 residues)
planarity	2.292	2251 non-hydrogen atoms

[a] Structure has been submitted to the Brookhaven Protein Data Bank under pdb1A7J.ent.

resolution. Once 60% of the residues were built, they were subjected to limited positional refinement. Phases from this partial model were calculated and combined with the original MIR phases and the resulting electron density map was subjected to solvent flattening. These phases were used to calculate a new map, additional alanine residues were added, and the process was reiterated. Alignment of the sequence to the polypeptide made use of the mercury position near cysteine 194, the platinum near histidine 193, and the platinum near histidine 167 as well as identifying bulkier residues like tryptophan. Interestingly, the third platinum site fell in the middle of a hydrophobic patch and likely represented noise from lack of isomorphism between the derivative and the native structure. Once the sequence was built into the electron density, it was possible to extend the resolution to 2.5 Å and use only the calculated phases. After a total of 36 rounds of manual rebuilding and refinement, the model had an R-value of 21.3% and a free R-value of 28.4% at a resolution of 2.5 Å (Table 2).

Description of the Structure. PRK is composed of a seven-stranded mixed β-sheet, with an auxiliary antiparallel pair of β-strands and seven α-helices (Figure 1). The amino terminus (residue 2) forms an odd interaction with residue 5 to form a "lariat" structure prior to the initial β-strand (1) (5−11). The β-strand enters into a disordered P-loop as predicted by sequence analysis (Walker A motif), followed by an α-helix (A) (21−32). After a turn, the structure forms a second parallel β-strand (2) (36−40), which is separated from β-strand 1 by β-strand 3 and is at the edge of the main β-sheet. The polypeptide chain forms a "random" coil region containing the conserved amino acid residues Asp 42, His 45, and Arg 49, identified as being part of the active site by mutagenesis (*9*). Arg 49 is actually the first residue of the second α-helix (B) (49−62), which leads into additional random coil followed by α-helix (C) (77−89). The first β-strand (1′) (93−96) that is not connected to the main β-sheet system follows, which is connected by a disordered random coil that leads into the second antiparallel β-strand (2′) (117−122). Now β-strand 3 containing the "Walker B motif" (127−132) runs parallel to and between β-strands 1 and 2. After some random coil and α-helix (D) (144−147), β-strand 4 (150−156) runs parallel to β-strand 1 and into the transverse α-helix (E) (158−171) and into some high-

temperature factor random coil back down helix F (180−193, 195−201) and the last parallel β-strand (5) (204−209). After some random coil, the first main sheet antiparallel β-strand (6) (230−235) leads into the short α-helix (G) (243−250) and the last main sheet antiparallel strand (7) (260−263), which leads to the carboxy-terminal α-helix (H) (268−288). A single sulfate molecule is bound to His 69, Arg 186, and Lys 165, which places this molecule about 12 Å from the disordered P loop. Residue Arg 186 forms a salt bridge with Glu 178 (2.7 Å), both of which are conserved in prokaryotes. The absolutely conserved Arg 187 forms a salt bridge with Glu 161 (2.6 Å), a residue conserved in prokaryotes, and the two absolutely conserved residues Lys 165 and Asp 169 also form a salt bridge (3.1 Å). The remaining active-site residues are not involved in salt bridges.

Structural Alignments. The program DALI (*18*) was used to find proteins that have a similar fold to PRK. DALI identified the structures of guanylate kinase (*19*), adenylate kinase (*20−22*), uridylate kinase (*23*), and *Hha*I DNA methylase (*24*) as being similar to PRK. Subsequently, we found that the structure of 6-phosphofructo-2-kinase (F6P 2K) (*25*), another phosphosugar kinase, is similar to PRK. By use of the least-squares minimization routines in the program O (*16*), the α-carbons of PRK, adenylate kinase (pdb1ak2.ent), guanylate kinase (pdb1gky.ent), and uridylate kinase (pdb1ukz.ent) were superimposed. Table 3 shows a composite structural alignment between the structures of PRK and adenylate kinase isozyme 2 with sulfate bound at the P-loop, guanylate kinase complexed with GMP and sulfate bound at the P-loop, and uridylate kinase with both ADP and AMP bound. There is no sequence similarity between PRK and the nucleotide monophosphate binding site of adenylate kinase. The tertiary structure of the ATP binding site and catalytic regions are highly homologous including secondary structural elements of β-strands 1−5 and α-helices A, E, F′, and H. This core region defines the nucleotide monophosphate kinase fold (*26*). Figure 2 shows the alignment of this core region of PRK with that of adenylate kinase. The Walker A sequence (12−20) or P-loop is disordered in the structure of PRK, while the Walker B sequence (129-FYEG) at the end of β-sheet 3 is well ordered. The phosphoryl acceptor region of PRK (composed of α-helices B and C and β-strands 1′ and 2′) is quite different
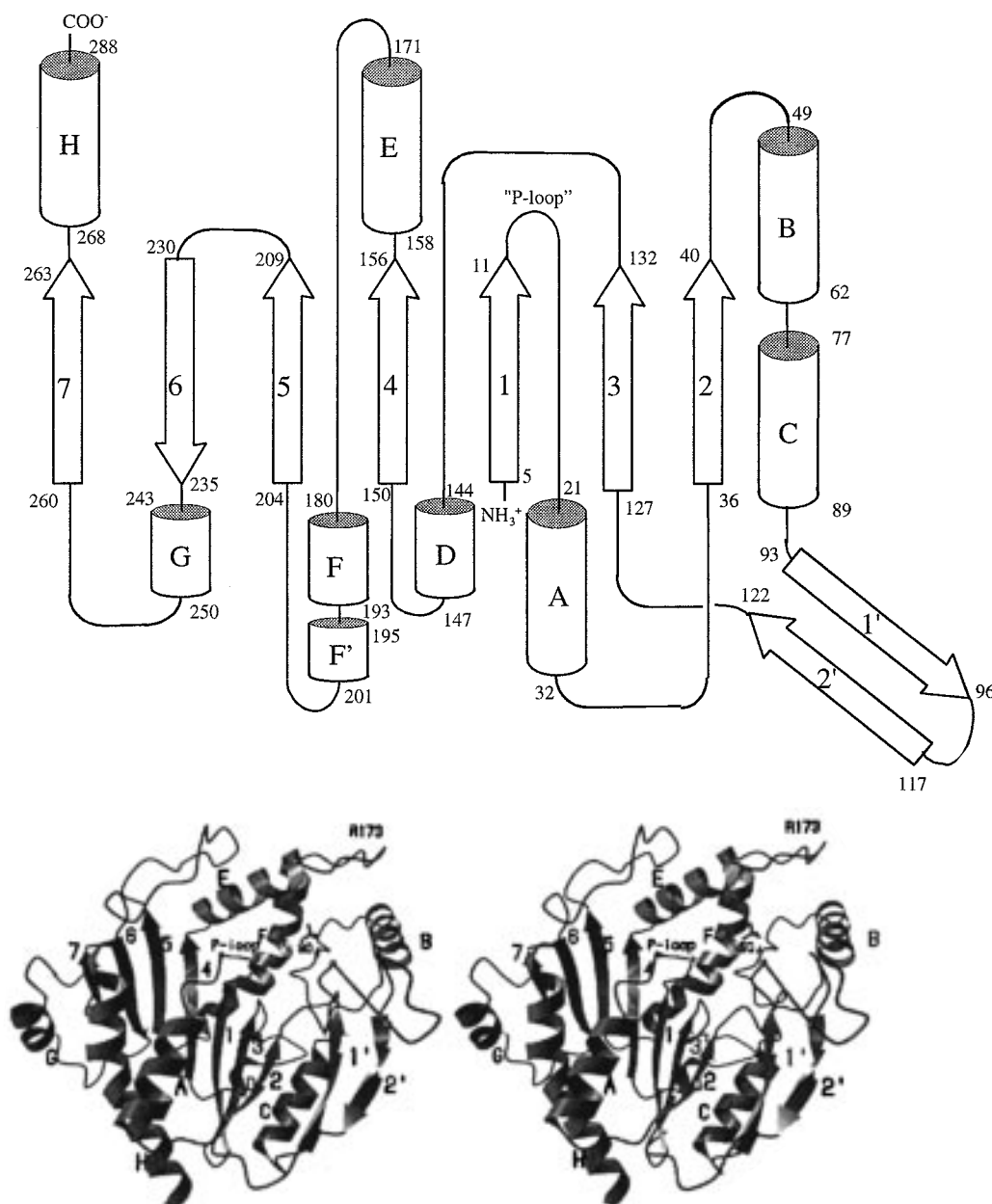
FIGURE 1: (a, top) Schematic diagram of the secondary structural elements that form phosphoribulokinase. (b, bottom) Stereo diagram of a PRK monomer with each secondary structural element labeled.

from the phosphoryl acceptor region of other nucleotide monophophate kinases. Differences in this region of the molecule are quite common among the nucleotide monophosphate kinase family. For example, the sulfuryl acceptor binding domain of the estrogen sulfotransferase enzyme (*27*) and the phosphoryl acceptor binding domain of phospho-fructo-2-kinase (*25*) do not resemble each other or the AMP binding domain of adenylate kinase. The remainder of the protein (β-strands 6 and 7 and α-helix G) is involved in protein–protein contacts with other monomers in the octamer and is not present in any of the other nucleotide monophosphate kinase family members.

Active Site of Phosphoribulokinase. On the basis of the structural similarity surrounding the P-loop among these proteins and the locations of conserved amino acids known to be important to catalysis, it is assumed that residues in the vicinity of the P-loop and the bound sulfate molecule form the active site of PRK. Site-directed mutagenesis data

are consistent with this conclusion (*9–11*). The active site is delineated by the main β-sheet, the P-loop that projects into the active site, and the three helices B, E, and F (Figure 3). The loop region between helices E and F may also be in the active site when substrate is bound.

Near the P-loop are the amino acids glutamic acid 131 and aspartic acid 42. Glutamic acid 131 is part of the Walker B sequence and is located on the β-sheet floor of the active site. Site-directed mutagenesis of aspartic acid 42 to alanine reduces catalytic efficiency by 100 000-fold (*9*), and this residue is located in a loop region that traverses the space between β-strand 2 and the α-helix B. Nearby is histidine 45, which affects the K_m of Ru5P (*10*) and is also part of the active-site cavity. Arginine 49, the first residue of α-helix B, also affects the K_m of Ru5P (*10*). One helical turn later, lysine 53 enters the active site. The loop between β-strands 1′ and 2′ is above the active site and both of the conserved residues, tyrosine 98 and histidine 100, are near

Table 3: Structural Alignment between Kinases[a]

```
PRK     4  AHPIISVTGSS----..STVKHTFDQIF---GVAAVSIEGDAFH      45
1ukz   15  QVSVIFVLG-------.TQCEKL-KDYS-......VHLSAGDLL        51
1gky    2   RPIVISGPS----..STLLKKLF-----..SFGFS               32
1ak2   16  --RAVLLG-------GTQA---KNFC......VCHLA               46


PRK    70  FSYE---LAELE       81
1ukz   73  GQIV-..QEITL       82


PRK   123  SASHLLFYEG        132
1ukz   95  ANKHKFLIDG        104
1ak2   94   KNGFLLDG         101


PRK   147  LADLKIGVVPVINLEWAQKIHRD        169
1ukz  121  ESKFILFFDCPEDIMLERLLERG        143
1gky  115  -RFLFIAPPSVEDLKKRLEGRG         136
1ak2  123   LDSVIEFSIPDSLLIR              138


PRK   189  HAYVHCIVPQFS......QTDINFQR        208
1ukz  161  NTFKETSMPVIE-------.VVRVRC        185
1gky  148  ----AELAYAE--.....AHDKVIVN        168
1ak2  190   AYHTQTTPLVE--------HSAIDA        213


PRK   267  KLDLAMQLILTPL     279
1ukz  191  DVYKDVQDAIR       201
1gky  173  KAYKELKDFIFAE     185
1ak2  219  VVFASIL           225
```

[a] PRK, phosphoribulokinase; 1ukz, uridylate kinase complexed with ADP and AMP, 1gky, guanylate kinase complexed with GMP and sulfate; 1ak2, adenylate kinase isozyme 2 with sulfate. Dashes represent sequences that do not align structurally; periods are for typographic registration.

the active site. In the middle of α-helix E, lysine 165 enters the active site. This lysine, together with arginine 186 and histidine 69 (part of a loop that follows α-helix B), binds to a sulfate ion located near the putative Ru5P phosphate binding site. Continuing up helix E is arginine 168; this residue points in the direction of the P-loop. Aspartic acid 169 has been implicated in the catalytic mechanism by site-directed mutagenesis and it points toward helix F. Arginine

173 is disordered and is located in the middle of the loop between helices E and F. Glutamic acid 178 makes a salt bridge to arginine 186. Arginine 187 (on helix F) points toward the P-loop and makes a salt bridge with the nonconserved glutamic acid 161.

Quaternary Structure. In the crystal, each unit cell contains 24 subunits arranged as three octamers each with 422 symmetry. Because bacterial PRK forms an octamer in solution (*2*), the crystallographic octamer is likely to be biologically relevant. The octamer has two layers with four PRK molecules on the top layer and four 2-fold rotated PRK molecules on the bottom layer displaced by about an eighth of a turn when viewed down the 4-fold axis of symmetry (Figure 4a). From this vantage point there appears to be an 8 Å hole in the center of the octamer that is defined by a "hub" composed of symmetry-related residues from α-helix G. The 2-fold symmetry that relates the top layer to the bottom layer has the effect of forming a right-handed "pinwheellike" structure, where each spoke consists of a dimer (Figure 4b,c). Each PRK monomer on the top layer makes contacts with the two monomers on its left and right, the monomer below and to the right, and the monomer below and to the left (e.g., the red monomer contacts the two yellow monomers, the blue monomer, and the green monomer). The area buried due to contact with the monomers on the left and right (e.g., the red with the two yellow monomers) is 640 Å², and there are no direct salt bridges between monomers. The area buried due to contact with the monomer below and to the right (e.g., the red with the green monomer) is 450 Å², and two salt bridges form between Asp 227 and Lys 267 and their 2-fold symmetric partners. The area buried due to contact with the monomer below and to the left (e.g., the red with the blue monomer) is 1760 Å². This represents a hydrophobic interaction of energy of between 38 and 44 kcal/mol (*28*). Furthermore, there are four salt bridges, one between Asp 213 and Arg 234 and a second between Glu 228 and Arg 257 and their respective 2-fold symmetric
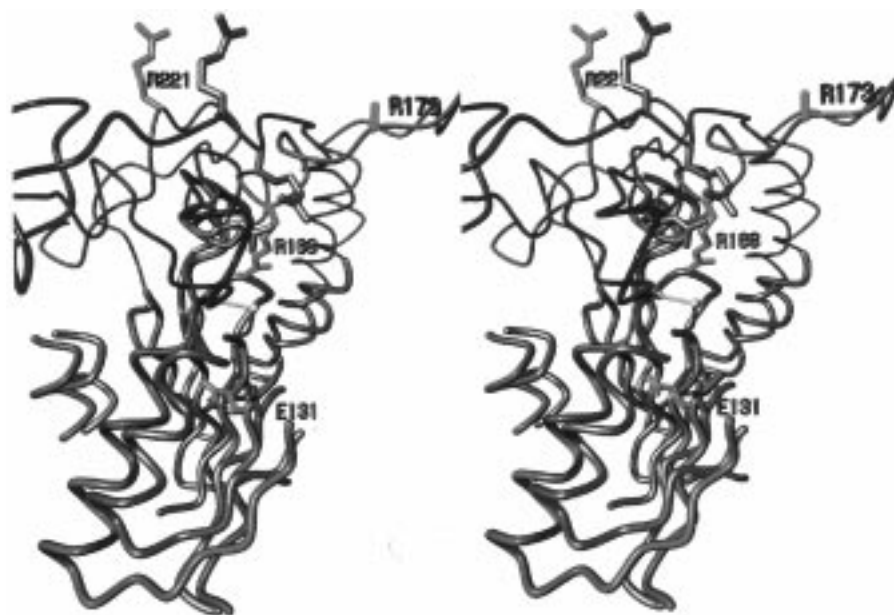

FIGURE 2: A superposition of the core structure (β sheets 1, 2, 3, 4, and 5, with α-helices A, E, F, and H) of phosphoribulokinase (red tones) and adenylate kinase (blue tones). The loop between β strands 5 and 6 is compared to the loop between α-helices E and F in adenylate kinase. Glutamic acid 131 of PRK was aligned with aspartic acid 100 of adenylate kinase. The program O was then used to optimize and superimpose the core structure with an overall rms deviation of 2.3 Å for the 67 pairs of α-carbons fit. Arginines known to interact with the phosphoryl groups of ATP bound to adenylate kinase are shown as are homologous arginines from PRK (labeled).
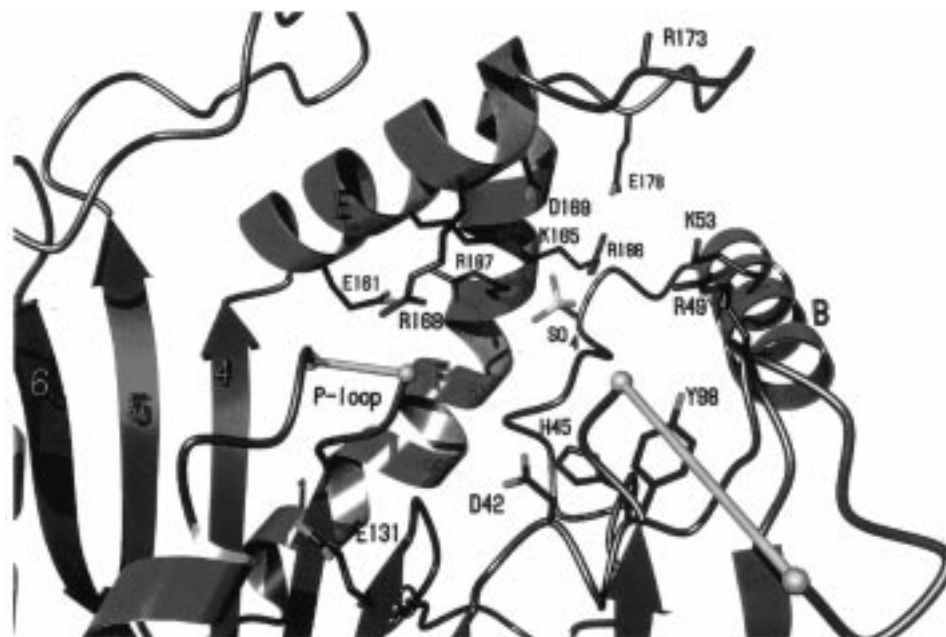
FIGURE 3: The active site of phosphoribulokinase with conserved residues shown. Note that Asp 42 and Asp 169 are found across the active site from each other. Asp 42 is not interacting with any other residue, while Asp 169 is engaged in a salt bridge with Lys 165 (3.1 Å). Lys 165 is in turn engaged in a salt bridge with the bound sulfate molecule (3.4 Å).
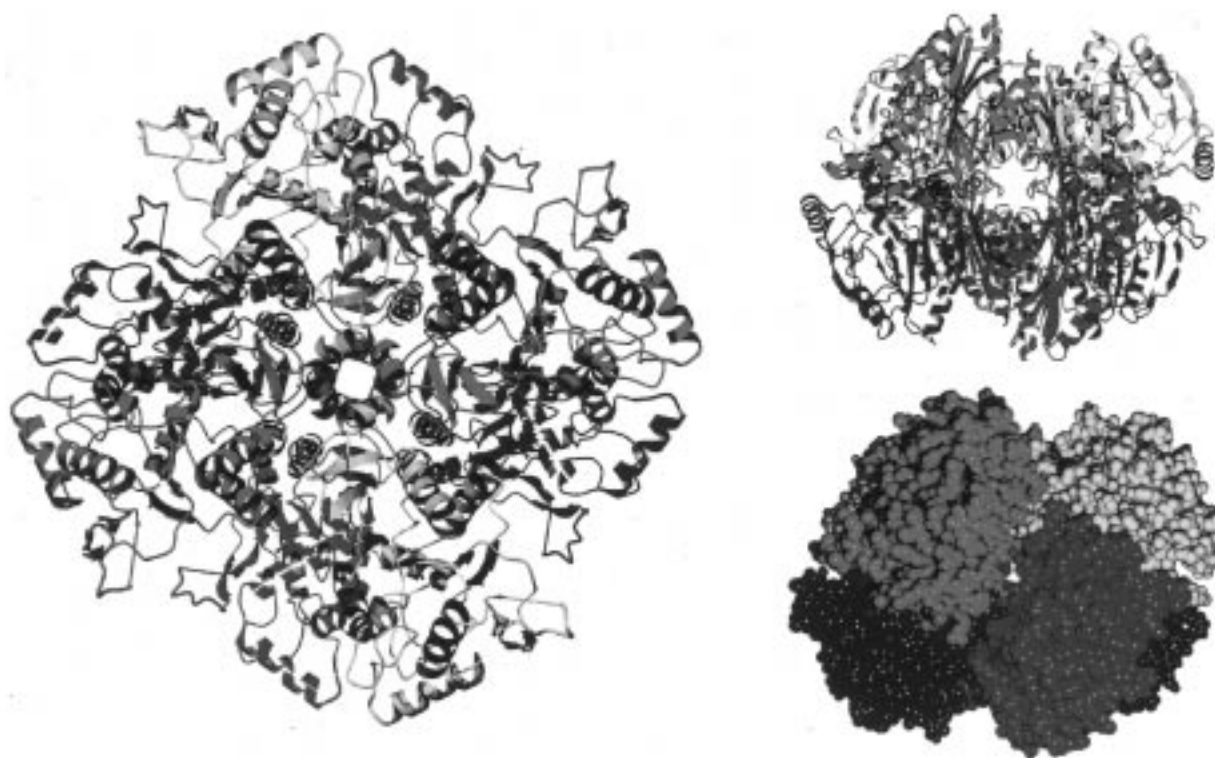

FIGURE 4: The phosphoribulokinase octamer (a, left) looking down the 4-fold axis of symmetry; (b, upper right) looking down a 2-fold axis of symmetry, the active site of the blue monomer is facing away, the green monomer is facing toward the viewer; (c, lower right) space-filling representation looking down the same 2-fold axis of symmetry; note the separation between the red and green monomers.

partners. Additionally, there exists a longer range (∼5 Å) electrostatic attraction between Asp 182 and His 193 and their respective 2-fold symmetric partners (Figure 5a). This dimer is now believed to be conserved throughout the evolution of PRK. The isolated monomer has a total solvent-accessible surface area of 14 180 Å². The fraction of surface area buried by the other subunits in the octamer is about 20% (4.5%, 3.2%, and 12.4%, respectively) or 2850 Å².

Docking Studies with Thioredoxin. Thioredoxin from the cyanobacteria *Anabaena* is believed to resemble the plant chloroplast type f thioredoxin used to regulate PRK (*29*). A structural model of this molecule was docked with the structure of PRK so that the cysteine residues 50 and 53 of thioredoxin were aligned with residues 16 and 40 of PRK. Two orientations (related by 180°) of thioredoxin could be fit into the active-site cavity of PRK. The width of the
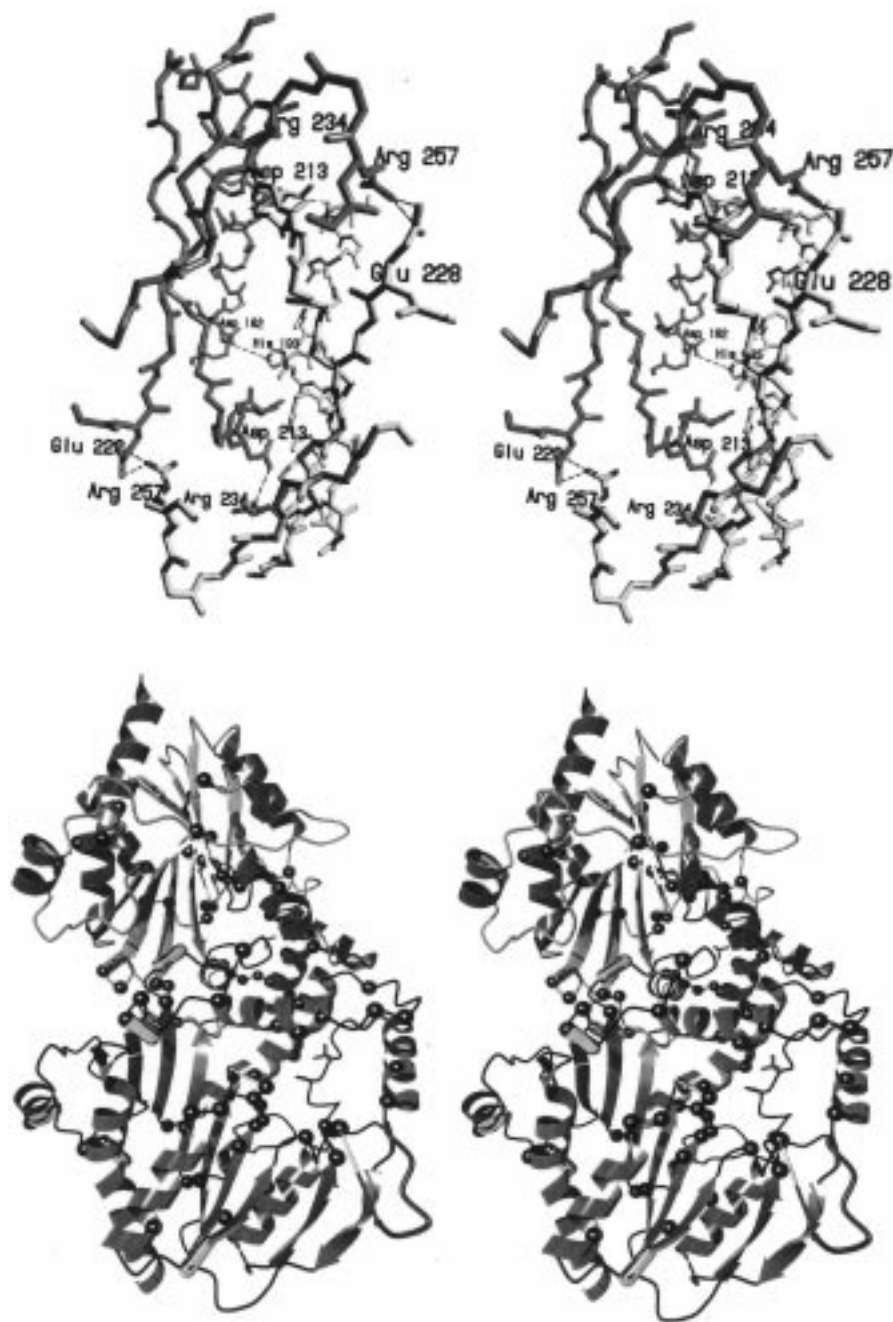
FIGURE 5: (a, top) Backbone representation of the large interface between the dimers believed to be conserved through evolution. The β-strands five, six, and seven and the α-helix F/F′ are involved in the formation of this interface. The three electrostatic interactions and their 2-fold symmetric partners are shown: Asp 182 and His 193, Asp 213 and Arg 234, and Glu 228 and Arg 257. (b, bottom) Ribbon drawing of the dimer believed to be conserved throughout evolution. A side view, looking nearly perpendicular to both the 2-fold axis of the dimer and the 4-fold axis of the octamer, the two helices on the far left of the figure form the inner core of the octamer. Monomer 1 consists of green α-helices, red β-strands, and black "random coil" regions, monomer 2 consists of magenta α-helices, yellow β-strands, and orange "random coil" regions. Blue regions indicate residues missing in eukaryotic PRKs but present in prokaryotic PRKs. Golden capsules represent areas of insertion in eukaryotic PRKs but absent in prokaryotic PRKs. The yellow balls-and-sticks represent regions of sequence which are not ordered the crystal structure. Black spheres are positioned at α-carbons of residues conserved throughout evolution. Note that most of these conserved residues cluster around the proposed active site.

active-site cavity of PRK matched the thickness of the thioredoxin molecule.

Mapping the Evolutionarily Conserved Residues. A sequence alignment of 12 PRK sequences from eukaryotic and prokaryotic species reveals that 44 different residues (about 15%) are highly conserved with two or fewer nonidentities (Table 4). Figure 5b maps all of the conserved residues and the insertion and deletion regions. Relative to the prokaryotic sequences, the eukaryotic sequences contain

three different deletion regions (in blue) and five different insertion regions (gold "capsules") and a longer carboxy terminus. One of the deletions appears to shorten the carboxy terminus of α-helix B and the other two regions are in "random coil" regions of the protein structure, one of them being disordered. The only two structural regions interrupted by insertions are α-helix G and the carboxy-terminal α-helix H. The insertion in α-helix G can be rationalized in that the eukaryotic proteins do not form

Table 4: Sequence of PRK from *Rhodobacter sphaeroides* A[a]

```
              1                                    35

              SSSSSSS "P-Loop" HHHH HHHHHHH

   rsPRKa    MSKKHPIISV TGSSGAGTST VKHTFDQIFR REGVK~~~~~


                     36                                    70

                     SSSS           HH HHHHHHHHH HHH

   rsPRKa    ~~~~~~~~~~ AVSIE GDAFHRFNRA DMKAELDRR YAAGDATFSH


        71                                             119

               HHH HHHHHHHHHH    SSSS     Disordered     SSS

   rsPRKa    FSYEANELKE LERVFREYGE TGQGRTRTYV HDDAEAARTG VAPGNFTDWR


        120                                            169

          SSS     SSS SSS         HHHH    SSSSSSS HH HHHHHHHHHH

   rsPRKa    DFDSDSHLLF YEGLHGAVVN SEVNIAGLAD LKIGVVPVIN LEWIQKIHRD


        170                    D                212      213

          HH          HHHHHHHHHH HHHH HHHHH HH SSSSSSS

   rsPRKa    RATRGYTTEA VTDVILRRMH AYVHCIVPQF SQTDINFQRV PVV~~~~~DT


        215        226          227              245     246

                                      SSSSSS        HH     HHHH

   rsPRKa    SNPFI ARWIPTA~~~ ~~~~~~~~DES VVVIRFRNPR GIDFPY~~~LTSM


        250                    275            276

          H           SSSS     HH HHHHH          HHHH

   rsPRKa    IHGSWMSRAN SIVVPGNKLD LAMQLI~~~~~ ~~~~~~~~LTPL


        280      290

          HHHHHHHHH

   rsPRKa    IDRVVRESKVA
```

[a] Residues conserved (90% identity) across the prokaryotic and eukaryotic kingdoms are shown in boldface type; residues conserved (100%) among bacterial species are shown in italic type. Underlined residues represent deletions, and tildes (~) represent insertions in the sequence of eukaryotic organisms. The boldface **D** in the numeric registration line represents a conserved aspartic acid in all species except *Rb. sphaeroides*. Lineups were made using GCG software (*44*) and the sequences of *Rb. sphaeroides* A and B (*45*), *Alcaligenes eutrophus* 1 and 2 (*46*), *Nitrobacter vulgaris*, *Xanthobacter flavus* (*47*), *Arabidopsis thaliana* (*48*), whtprk, *Mesembryanthemum crystallinum*, *Spinacea oleracea* (*49, 50*), *Chlamydomonas reinhardtii* (*51*), and *Synechocystis* (*52*).

octamers, and this helix is involved in octamer formation.

The three-dimensional distribution of highly conserved residues (black balls in Figure 5b) maps to three areas of the protein. The first region is found around the P-loop; this includes all of the residues that have been mutated and shown to play a role in catalysis (D42, H45, R49, E131, R168, D169, R173, and R187). Because the P-loop is known to bind the α and β phosphates of ATP in other P-loop-containing proteins, it is likely that this region is conserved due to its direct participation in catalysis (Figure 3). The second region of high sequence conservation is located between two monomers within the octamer; this interface is believed to define the dimer conserved throughout evolution. There are no absolutely conserved pairs of residues that make other protein−protein contacts with other monomers, although the absolutely conserved residue Asp 227 makes a salt bridge to a nonconserved Lys 267 in a third monomer. This is in contrast with those amino acids that are conserved only among bacterial PRKs, where contacts in all three possible monomer−monomer associations are conserved. The third region of high sequence conservation is near α-helix G, which forms the opening to the center of the octamer. These residues help to form the hydrophobic interior of the protein.

DISCUSSION

Likely Mechanism of Action. Since this crystal structure is in the "open" form and contains neither of the two substrates nor any inhibitors, it is not possible to make direct observations as to which residues are important for catalysis. However, it is possible to compare this structure to other known enzymes in the adenylate kinase family and to use mutagenic and kinetic data to form hypotheses for future testing. There are a variety of structures from the adenylate kinase family with a variety of substrates and inhibitors bound from which we can form some general hypotheses (*19–23, 30–35*). The overall picture is consistent with a mobile ATP binding "lid" and a NMP binding "lid" closing on each respective substrate upon binding to form a watertight seal that allows efficient phosphoryl transfer to occur. However, the individual amino acid residues that participate in both charge stabilization and substrate recognition are often quite different from family member to family member. Unlike the better characterized nucleotide monophosphate kinases, PRK, estrogen sulfotransferase, and F6P 2K need to both activate the phosphoryl (sulfuryl) acceptor and stabilize the pentacoodinate transition state. These enzymes are likely to follow the same general scheme with variations in the roles of individual amino acid residues.

On the basis of the structures of the nucleotide monophosphate kinases, it is expected that the structure of PRK will undergo significant conformational changes upon binding to substrate molecules. It is expected that upon binding ATP, residues in the P-loop, helix E, and helix F will have a number of interactions with the β- and γ-phosphate oxygens. On the basis of the movements observed in adenylate kinase, the movement of the loop between helices E and F may be greater than 10 Å upon ATP binding. In adenylate kinase and guanylate kinase the large loop between helices E and F interacts specifically with the adenosine ring, and these enzymes are specific for ATP. The size of the loop between helices E and F in PRK (170–178) is similar to that of F6P 2k and uridylate kinase. The crystal structures of F6P 2K (*25*) and uridylate kinase (*23*) reveal few protein interactions with the adenosine ring, and the authors hypothesize that under certain physiological circumstances GTP may act as the phosphoryl donor. Consistent with the shorter loop, it has been shown that bacterial PRKs can use various NTPs as phosphoryl donors (*2*). It is expected that there may be additional movements in the region surrounding α-helices B and F associated with ribulose 5-phosphate binding. As mentioned above, the loop between helices E and F could also move in response to ribulose 5-phosphate. It is also possible that the presently disordered loop residues between strands 1′ and 2′ may become ordered and help to recognize ribulose 5-phosphate. However, many of these residues in this loop are missing in the eukaryotic molecule, making it unlikely that they participate directly in binding. One of the challenges presented by this structure and the F6P 2K structure is determining how the phosphoryl acceptor substrate binds to the enzyme.

Catalytically Important Residues. The putative magnesium ligand from the Walker B sequence is a glutamic acid instead of the more usual aspartic acid. This may suggest a novel mode of binding for Mg·ATP to the active site of PRK. Site-directed mutagenesis of carboxylic acid residues in PRK suggests that there are two other carboxylate-bearing residues (Asp 42 and Asp 169) that may play a significant role in catalysis. Mutation of either of these residues reduces k_{cat} by 4–5 orders of magnitude (*9*); however, both mutants are able to bind ATP analogues with a stoichiometry of about 1, suggesting that both mutant enzymes are properly folded (*36*). This observation suggests that PRK has a base to activate the sugar oxygen. By contrast, the results of mutagenesis on aspartic acid residues in the structurally similar protein F6P 2K (*37*) were unable to identify a catalytic base to polarize the 2-hydroxyl of the hemiketal of fructose 6-phosphate.

In the crystal structure, Asp 42 is freely pointed toward the active site (as is Glu 131), while Asp 169 forms a salt bridge with Lys 165. Given the proximity of Asp 42 to Glu 131, it is tempting to speculate that Asp 42 also participates in magnesium binding. However, a number of different ATP and GTP binding proteins similar to PRK contain a negatively charged amino acid residue in the position of Asp 42 at the end of β-strand 3 (*7*). Little has been demonstrated about the function of this negatively charged amino acid in these other proteins, so it is not possible to make any direct comparisons, other than to note that in the X-ray structure this residue is never observed binding to the magnesium ion. However, the presence of a glutamic acid in the Walker B sequence, instead of the preferred aspartic acid, may alter the location of the magnesium site relative to other family members and allow Asp 42 to act as a direct or water-mediated magnesium ligand. Since the equivalent of Asp 169 is not found in other similarly folded enzymes, it is possible that it acts as the catalytic base. This, however, would contradict the recently proposed mechanisms for both thymidine kinase from herpes simplex virus and mouse estrogen sulfotransferase (*27, 38*). In these two enzymes, a residue (Glu 83 or His 108, respectively) positioned homologously to Asp 42 is involved in the polarization of the substrate hydroxyl group to be phosphorylated or sulfonated. Following this precedent, Asp 169 may either act as an additional ligand for the magnesium ion or simply function to position and neutralize the charge of Lys 165.

The identification of residues involved in the stabilization and coordination of the pentacoordinate transition state has been more difficult. In the nucleotide monophosphate kinase family an arginine in the loop between helices E and F participates in binding the γ-phosphoryl of ATP, often stabilizing the transition state. On the basis of homology with the residues Arg 142 and Arg 148 of uridylate kinase, it is expected that both of the arginines, Arg 168 and Arg 173, respectively, in PRK interact with the γ-phosphoryl of ATP. Although many mutations of conserved positively charged residues show an effect on the K_m of Ru5P, to date the results of this mutagenesis show only one residue (Arg 168) to have an effect (about 300-fold) on k_{cat} (*11*). The movement necessary for Arg 168 to bind the γ-phosphoryl of ATP could be sufficient to bring the carboxylate of the conserved Asp 169 to a position that would allow it to either polarize the O1 oxygen for attack on ATP or act as a ligand for the magnesium ion. This movement would position the disordered Arg 173 to bind either the γ-phosphate of ATP or the 5-phosphate of Ru5P. The effect of mutagenesis on Arg 173 yields only a 100-fold elevation in K_{Ru5P} (*11*). The simplest interpretation of this result would be that Arg 173

binds the 5-phosphate of Ru5P. However, if the stabilization of the transition state is not (partially) rate-determining in the mutant, it is possible that this effect on the apparent K_m is a result of a retarded, but "masked", catalytic step. In adenylate kinase the arginine at the position corresponding to Arg 173 has been shown to be responsible for stabilizing the pentacoordinate transition state. While there are still conserved positively charged residues in PRK that have not been subject to mutagenesis, it is difficult to imagine that these residues alone are responsible for the stabilization of the transition state. Since the identity of the residue responsible for stabilizing the transition state is not the same among NMP kinases, other residues should be considered. Certainly the conserved Lys 165 (for which there are no mutagenic data available to date) must be considered for this role. A crystal structure of PRK bound to a transition-state analogue would greatly help to resolve this issue.

Relationship of the Bacterial Enzyme to the Plant Enzyme. Although chloroplasts are thought to have originated as bacterial symbiotes of a eukaryotic host, the structural relationship between the bacterial and plant forms of PRK have been obscured through differences in quaternary structure, primary structure (sequence), and regulatory mechanism. However, the tertiary structure of a bacterial PRK reveals that a number of residues in the active-site region of the protein are identical or highly conserved across kingdoms. The extent of this conservation among the kingdoms is manifest by the fact that the size of the active site of the bacterial enzyme is large enough to fit an oriented molecule of thioredoxin, the molecule that regulates the activity of the plant enzyme. Interestingly, steric hinderence due to the octameric structure of the bacterial enzyme would prohibit the binding of thioredoxin to its active site. The aforementioned conserved eukaryotic dimer would be free to bind thioredoxin. The mechanism by which thioredoxin regulates the eukaryotic enzyme can be deduced by looking at the structure of the P-loop. Although the P-loop itself is disordered, it is constrained by good electron density for residues 12 and 18. The α-carbons of the disordered Ala 16 and Glu 40 are within 15 Å of each other in this bacterial model (Figure 3). To achieve a disulfide bridge in the eukaryotic enzyme, the two cysteine residues at these positions would need to move at least 5 Å, distorting the P-loop and making it incapable of productively binding ATP. Interestingly, unlike other P-loop-containing kinases, the P-loop of bacterial PRK does not contain a characteristically conserved lysine residue at position 18 but instead has a threonine residue. Other major differences in PRK sequences probably correlate with the differences in regulatory mechanism.

Possible Effects from Insertions and Deletions. Other than differences in sequence, there are five insertions and three deletions in the plant enzyme relative to the bacterial enzyme (Table 4, Figure 5b). Some of these insertions and deletions may have significant implications in the context of the divergence of the two kingdoms. However, the insertions before β-strand 2 and in the middle of α-helix H are unlikely to make a contribution to either enzyme activity or regulation as they are far from the active site or known protein−protein interfaces. A three-residue insertion that may play a role in the prevention of octamerization is found in helix G, which is in the tightly packed core of each of the two tetramers

that form the octamer. This insertion may extend helix G and make octamer formation impossible. Interestingly, Tyr 245 in helix G is absolutely conserved and helps to pack this helix onto the core structure. It is possible that this helix serves a similar role in the plant enzyme, facilitating protein−protein contacts with other enzymes involved in the Calvin cycle. There have been some reports of plant PRKs involved in multienzyme complexes (*39, 40*).

Two additional insertions (5 and 11 residues) found in the plant enzyme are both in the loop between β-strands 5 and 6. As these inserted residues are near the conserved dimer interface, they may act to increase either the number of specific interactions or intermolecular hydrophobic contacts with the other monomer. However, this ignores the fact that the loop between strands 5 and 6 has two conserved residues, Arg 221 and Asp 227, that are not in contact with with the other monomer or active site but simply pointed toward the solvent. The only residue in this loop making significant contact with another monomer is at the carboxy-terminal end of the loop. The conserved Glu 228 makes an intermolecular salt bridge with Arg 257 in the dimer conserved in evolution. An alternative hypothesis for the function of this loop and the additional residues inserted into the eukaryotic sequence may be derived from examining the open and closed structures of adenylate kinase (*41−43*). The relative location of Arg 221 in PRK is similar to that of Arg 143 in AK in the "open" structure, although this arginine is about 10 Å further from the P-loop than in adenylate kinase (Figure 2). Upon binding ATP, this arginine in adenylate kinase moves 10 Å to bind the β-phosphoryl and γ-phosphoryl of ATP and promotes catalysis. In PRK, Arg 221 may perform the same role. The loop may move to allow the guanidinium group to interact with the phosphoryls of ATP. One may hypothesize that the additional residues found in the loop of the eukaryotic enzyme may be due to the fact that the eukaryotic enzyme is not allosterically regulated.

Two bacterial specific insertions, a loop between β-strands 1′ and 2′ and another loop following α-helix B, are in three-dimensional proximity to Arg 186 and Glu 178 and may contribute to the allosteric regulation of the bacterial protein. In the presence of NADH, mutation of Arg 186 eliminates allosterism in ATP binding, reducing the Hill coefficient from 1.8 to 1.0 (*11*). Mutation of glutamic acid 178 to alanine reduces the stimulation by NADH from 37-fold for the wild-type enzyme to 9-fold in the mutant (*9*). There are no mutagenic data for the contributions of either additional bacterial loop to allosteric regulation of the bacterial enzyme. The remainder of the active-site residues that are likely to be in contact with the substrates are identical for the two kingdoms.

Positive Charges and the Quaternary Structure. The quaternary structure of the enzyme positions the catalytic face of each monomer containing the P-loop facing the inverted P-loop of the adjacent monomer (the active sites of the red and green monomers in Figure 4). A number of positively charged amino acid residues are found on this face of the protein and give rise to the positive electrostatic potential between the monomers. An ATP molecule binding to one active site might influence the binding of ATP to the other active site by an electrostatic mechanism. Further, a number of positively charged amino acid residues are localized on the backside of the β-sheet, near Arg 221, in

the region between the conserved dimer (red and blue monomers in Figure 4) and a third monomer (green monomer in Figure 4). This positively charged region may provide a binding site for the negatively charged positive and negative allosteric effectors NADH and AMP. There is no classic Rossmann fold to be identified as the NADH binding site. It is possible that binding NADH could cause a conformational shift in the bacterial PRK that would change its ATP binding characteristics. Given the location of this putative site, changes in conformation in one monomer could be transmitted throughout the octamer.

It has been shown that, in the absence of NADH, PRK interacts with ATP and ATP analogues to form binary complexes from which the nucleotide exchanges very slowly (*36*). We also reported the formation of stable ternary complexes of PRK with NADH and adenine nucleotide (*36*). Recently, we have characterized these complexes in more detail and confirmed the formation of PRK·NADH·trinitrophenyl-ATP and PRK·NADH·ATP complexes. The data prompt a refinement of our earlier report (*36*) to reflect the observation that ATP exchanges from a ternary complex more rapidly than does trinitrophenyl-ATP. Thus, a stoichiometric PRK·NADH·ATP complex is not stable to centrifugal gel filtration. Such observations are consistent with a conformational change in the enzyme which allows more rapid ATP exchange from the ternary complex that includes NADH. Clearly, a X-ray structure of the enzyme bound to NADH would help in addressing this issue.

Conclusions and Future Experiments. This first structure of PRK from *Rb. sphaeroides* provides a new framework for thinking about the catalytic mechanism, PRK's place in the evolution of kinases, and the relationship of the bacterial to the eukaryotic enzyme. To identify roles for specific amino acid residues in substrate binding, catalysis, and product release, it will be necessary to crystallize and determine the structure of PRK bound to a variety of substrates (Mg^{2+}·ATP, Ru5P), inhibitors, and allosteric regulators (NADH, AMP). The use of more sophisticated spectroscopic and kinetic experiments would also be useful in this regard. Mutagenic studies that switch prokaryotic sequences for eukaryotic sequences may be useful in analyzing the basis for regulatory differences. Work is currently being pursued in all of these different areas.

REFERENCES

1. Miziorko, H. M., and Eckstein, F. (1984) *J. Biol. Chem. 259*, 13037−13040.
2. Siebert, K., Schobert, P., and Bowien, B. (1981) *Biochim. Biophys. Acta 658*, 35−44.
3. Tabita, F. R. (1980) *J. Bacteriol. 143*, 1275−1280.
4. Buchanan, B. B. (1980) *Annu. Rev. Plant Physiol. 31*, 341−374.
5. Krieger, T. J., and Miziorko, H. M. (1986) *Biochemistry 25*, 3496−3501.
6. Porter, M. A., Potter, M. D., and Hartman, F. C. (1990) *J. Protein Chem. 9*, 445−451.
7. Saraste, M., Sibbald, P. R., and Wittinghofer, A. (1990) *Trends Biochem. Sci. 15*, 430−434.
8. Milanez, S., Mural, R. J., and Hartman, F. C. (1991) *J. Biol. Chem. 266*, 10694−10699.
9. Charlier, H. A., Jr., Runquist, J. A., and Miziorko, H. M. (1994) *Biochemistry 33*, 9343−9350.
10. Sandbaken, M. G., Runquist, J. A., Barbieri, J. T., and Miziorko, H. M. (1992) *Biochemistry 31*, 3715−3719.
11. Runquist, J. A., Harrison, D. H. T., and Miziorko, H. M. (1998) *Biochemistry 37*, 1221−1226.
12. Roberts, D. L., Runquist, J. A., Miziorko, H. M., and Kim, J. J. (1995) *Protein Sci. 4*, 2442−2443.
13. Otwinowski, Z., Minor, W., and Gewirth, D. (1993) in *The HKL Manual*, Yale University Press, New Haven, CT.
14. McRee, D. (1997) *Mol. Graphics 10*, 44−46.
15. Collaborative Computational Project No. 4 (1997) *Acta Crystallogr. D50*, 760−763.
16. Jones, T. A. (1991) *Acta Crystallogr. A47*, 110−119.
17. Brünger, A. T. (1993) in *X-PLOR Version 3.1 Manual*, Yale Unversity Press, New Haven, CT.
18. Holm, L., and Sander, C. (1993) *J. Mol. Biol. 233*, 123−138.
19. Stehle, T., and Schulz, G. E. (1992) *J. Mol. Biol. 224*, 1127−1141.
20. Diederichs, K., and Schulz, G. E. (1990) *Biochemistry 29*, 8138−8144.
21. Dreusicke, D., Karplus, P. A., and Schulz, G. E. (1988) *J. Mol. Biol. 199*, 359−371.
22. Muller, C. W., and Schulz, G. E. (1988) *J. Mol. Biol. 202*, 909−912.
23. Muller-Dieckmann, H. J., and Schulz, G. E. (1994) *J. Mol. Biol. 236*, 361−367.
24. Cheng, X., Kumar, S., Posfai, J., Pflugrath, J. W., and Roberts, R. J. (1993) *Cell 74*, 299−307.
25. Hasemann, C. A., Istvan, E. S., Uyeda, K., and Deisenhofer, J. (1996) *Structure 4*, 1017−1029.
26. Schulz, G. E., Schiltz, E., Tomasselli, A. G., Frank, R., Brune, M., Wittinghofer, A., and Schirmer, R. H. (1986) *Eur. J. Biochem. 161*, 127−132.
27. Kakuta, Y., Pedersen, L. G., Carter, C. W., Negishi, M., and Pedersen, L. C. (1997) *Nat. Struct. Biol. 4*, 904−908.
28. Creighton, T. E. (1984) in *Proteins: Structures and Molecular Properties* (Anonymous) pp 133−198, W. H. Freeman and Company, New York.
29. Saarinen, M., Gleason, F. K., and Eklund, H. (1995) *Structure 3*, 1097−1108.
30. Wild, K., Bohner, T., Aubry, A., Folkers, G., and Schulz, G. E. (1995) *FEBS Lett. 368*, 289−292.
31. Schlauderer, G. J., Proba, K., and Schulz, G. E. (1996) *J. Mol. Biol. 256*, 223−227.
32. Muller, C. W., and Schulz, G. E. (1992) *J. Mol. Biol. 224*, 159−177.
33. Diederichs, K., and Schulz, G. E. (1991) *J. Mol. Biol. 217*, 541−549.
34. Stehle, T., and Schulz, G. E. (1990) *J. Mol. Biol. 211*, 249−254.
35. Schlauderer, G. J., and Schulz, G. E. (1996) *Protein Sci. 5*, 434−441.
36. Runquist, J. A., Narasimhan, C., Wolff, C. E., Koteiche, H. A., and Miziorko, H. M. (1996) *Biochemistry 35*, 15049−15056.
37. Bertrand, L., Deprez, J., Vertommen, D., Di Pietro, A., Hue, L., and Rider, M. H. (1997) *Biochem. J. 321*, 623−627.
38. Wild, K., Bohner, T., Folkers, G., and Schulz, G. E. (1997) *Protein Sci. 6*, 2097−2106.
39. Clasper, S., Easterby, J. S., and Powls, R. (1991) *Eur. J. Biochem. 202*, 1239−1246.
40. Rault, M., Giudici-Orticoni, M. T., Gontero, B., and Ricard, J. (1993) *Eur. J. Biochem. 217*, 1065−1073.
41. Schulz, G. E., Elzinga, M., Marx, F., and Schrimer, R. H. (1974) *Nature 250*, 120−123.
42. Egner, U., Tomasselli, A. G., and Schulz, G. E. (1987) *J. Mol. Biol. 195*, 649−658.
43. Muller, C. W., Schlauderer, G. J., Reinstein, J., and Schulz, G. E. (1996) *Structure 4*, 147−156.
44. Genetics Computer Group (1982) *GCG Wisconsin Package*, University of Wisconsin, Madison, WI.

45. Gibson, J. L., Chen, J. H., Tower, P. A., and Tabita, F. R. (1990) *Biochemistry 29*, 8085−8093.

46. Kossmann, J., Klintworth, R., and Bowien, B. (1989) *Gene 85*, 247−252.

47. Meijer, W. G., Enequist, H. G., Terpstra, P., and Dijkhuizen, L. (1990) *J. Gen. Microbiol. 136*, 2225−2230.

48. Horsnell, P. R., and Raines, C. A. (1991) *Plant Mol. Biol. 17*, 183−184.

49. Milanez, S., and Mural, R. J. (1988) *Gene 66*, 55−63.

50. Roesler, K. R., and Ogren, W. L. (1988) *Nucleic Acids Res. 16*, 7192.

51. Roesler, K. R., and Ogren, W. L. (1990) *Plant Physiol. 93*, 188−193.

52. Su, X., and Bogorad, L. (1991) *J. Biol. Chem. 266*, 23698−23705.